This manuscript is a pre-print and has not undergone peer review. We welcome any feedback.

Dynamic Mode Decomposition for Analyzing Dynamics in Multi-phase Flow in Porous Media

Catherine Spurin,* Ryan Armstrong, James McClure, and Steffen Berg

Abstract

For multi-phase flow through multi-scale heterogeneous porous media, such as the pore space of rocks, the interaction between multiple immiscible fluids and an intricate network of pores, creates a wide range of dynamic flow phenomena. At larger scales i.e. scales relevant for practical applications such as carbon sequestration, this interplay of dynamic phenomena is often referred to as "complexity". However, it is important to describe the persistent features of the flow in an adequate manner, to represent the "complexity" of the system. Dynamic mode decomposition (DMD) is a dimensionality reduction algorithm that computes a set of modes associated with fixed oscillatory behaviours. In this work, data is extracted from dynamic two-phase flow experiments and analzed with DMD. We show that DMD can reproduce the data. Furthermore, not all dynamic modes are required to reproduce key dynamic features; this highlights the important spatial and temporal scales for flow. We show that dynamic mode decomposition was able to identify localized regions important to flow. Overall, DMD is proven as a useful diagnostic tool for complex 4D flow dynamics for multi-phase flow.

* cspurin@stanford.edu

I. INTRODUCTION

Multiphase flow in porous media is subject to complex dynamics caused by the interaction of multiple immiscible fluid phases with a heterogeneous pore space. This leads to a complicated sequence of displacements governed by the interplay of capillary, viscous, inertial and gravity forces. Historically, attempts have been made to decompose the dynamics into a limited set of elementary fluid configurations, displacement mechanisms etc. that would allow one to develop intuitive and practical models to upscale pore scale dynamics to the relevant (for most applications) Darcy scale [1, 2]. Lenormand made a breakthrough by identifying 4 distinct elementary displacement mechanisms in micromodel experiments [3]. While these 4 elementary mechanisms are still being actively used for instance in quasi-static pore network modelling [4–6], there are many dynamic phenomena such as the impact of inertial forces which are not captured in these concepts [7]. This shortcoming was addressed by the decomposition of *dynamic* flow phenomena into connected pathway flow and ganglion dynamics [8, 9]. While instructive, this work mainly led to the insight that asymmetries in pore-scale displacement dynamics are an important cause for hysteresis [10].

The well-established foundations of statistical physics and thermodynamics addresses the macroscopic behavior of systems with many internal degrees of freedom. That is, in principle, also the case for multiphase flow in porous media, where one can regard the pore-scale configurations of immiscible fluids as internal degrees of freedom. The first step is to identify the macroscopic state variables. The second is to describe the dynamics of the system. It has been shown that, in multiphase flow in porous media, the capillary state function can be represented by the 4 Minkowski functionals [11]. This is a direct consequence of Hadwiger's theorem [12] in integral geometry, which states that any linear, additive property of an object in 3D can be represented though linear combinations of the 4 Minkowski functionals, which are (1) volume, (2) interfacial area, (3) mean curvature, and (4) the Gaussian curvature [13].

The 4 Minkowski functionals represent a complete set of state variables which demonstrates that the historical view of capillary pressure hysteresis, i.e. the path dependency (drainage vs. imbibition) is an artifact of an insufficient set of state variables [10, 14, 15]. Note that the hysteresis introduced by an alteration of the wetting properties e.g. at the end of the drainage state is real, which can also be addressed with the integral geometry

approach [16].

While the discovery of the geometric state function is a major breakthrough for advancing the understanding and formulation of multiphase flow in porous media, it is still difficult to make a direct step from the state function to transport equations. Even though the geometric state function is universal i.e. holds for static and dynamic situations, there are several complications associated with transport. First, the link between phase pressure difference and mean curvature i.e. Laplace pressure is strictly valid only for equilibrium or at least quasi-static situations [17]. But that is not the case anymore during flow, meaning that the phase pressure difference, which is an essential variable for the for formulation of transport, is not given by an equilibrium interface curvature anymore, i.e. is not covered by the 3$^{\text{rd}}$ Minkowski functional. Furthermore, transport is generally a superposition of fluid flow within individual phases and fluid-fluid *displacements*. Fluid-fluid displacements which are often highly non-linear, and in addition to viscous and capillary forces also involve inertial forces [7], change phase saturation and also fluid topology, i.e. the state of the system [10]. That occurs on the scale of individual pores to fluid clusters which spans a range of length scales typically 4 or more orders of magnitude [5]. The collective global dynamics where local equilibrium states are activated by fluid-fluid displacements and then change or interact via mechanisms such as ganglion dynamics [8], results in highly complex spatio-temporal sequences with an associated range of relaxation times from seconds [18] to hours [19]. From the complex spatio-temporal dynamics which is multi-scale in space and time, macroscopic flow regimes emerge that range - depending on conditions - from connected pathway flow to ganglion dynamics [8, 9, 20]. Unless we are able to predict the toplogical changes caused by these flow regimes, and its associated macroscopic averages, it is difficult to advance the description level from the state function to transport equations and to make a connection between pore and Darcy scale dynamic phenomena.

Because of these conceptual complications, historically, at the Darcy scale the predominant formulation for multiphase transport equations is a phenomenological extension of Darcy's law [21] from single to multiphase flow. There are a number of extensions that capture some of the state variables such as interfacial area [22]. Also, extensions that honor the connection between relative permeability and fluid topology [23] in a phenomenological manner exist [24]; however, a rigorous derivation of the geometric state function for dynamic phenomena / flow and transport in a first-principles causal manner is currently lacking.

For bottom-up upscaling, starting with the evolution of the geometric state [17], difficulties were encountered because discontinuous pore-scale displacement events propagate via the Minkowski-Steiner formula [11] through the Minkowski functionals. This leads to non-differentiable state variables [25] which would imply ultimately a non-differentiable Euler-Lagrange function (although Hansen *et al.* were able to circumvent that problem by assuming an equal probability for each capillary state in the partition function [26]). However, most of the recent literature highlighting complex dynamics at pore-scale with topological changes of fluid-fluid interfaces, even at steady-state conditions. The fluctuations in saturation and pressure could provide an indication to connectivity and wettability [9, 27–30].

Fluctuations have previously been considered noise [27, 30–32]. However, it has been observed with X-ray imaging, that there is a link between fluctuations in saturation and pressure measurements and pore-scale displacement events [20]. Rücker *et al.* [27] identified that fluctuations are instability modes, where the unstable mode provides, at the same pressure drop, a higher total flux.

To avoid the difficulties that arise with the more conventional upscaling, and taking the fluctuation dynamics into account, a different method for upscaling was chosen which starts at the fluctuations observed in most fractional flow experiments [20, 27] and defining the energy dynamics by space-and-time averages [33, 34]. It has been demonstrated that the two-phase Darcy equation can be rigorously derived for stationary conditions ("steady-state") where the *collective* energy dynamics of *all* fluctuations *together* averages out [35]. Individual properties such as pressure still show significant fluctuations also at large length scales but the collective behaviour of the energy dynamics over a long enough time scale provide a steady-state condition.

Here we follow the idea of regarding fluctuations as instability modes [27] that connect pore scale dynamics with macroscpic flow regimes. The dissipation of the system is linked to the fluctuations via the fluctuation-dissipation theorem which is also applicable to multi-phase flow in porous media [36, 37]. Depending on the fractional flow, f_w, (and potentially also the fractional flow history) the fluctuations can be irregular, or periodic with large amplitudes, which points potentially to a non-linear resonance phenomenon with observations that could be interpreted as frequency doubling or bifurcations.

The potential connection between resonant modes of the stochastic fluctuations and the Pollicott-Ruelle resonances [38, 39] provided the motivation to investigate whether a direct

connection can be established between the modes obtained in Dynamic Mode Decomposition (DMD) and their dynamics of spatio-temporal data of fluctuations and the capillary state.

The remaining challenge is to understand the origin and structure of the fluctuations, and predict the fluctuation spectrum. This would open a route to predicting relative permeability via the fluctuation-dissipation theorem, without running an experiment, or conducting a pore scale flow simulation, which are both time consuming and expensive [40]. Therefore, in this paper, we address the problem of gaining deeper insights into the origin of the fluctuations using DMD.

II. DYNAMIC MODE DECOMPOSITION (DMD)

DMD has been largely developed in the domain of fluid mechanics [41] and applied, for instance, to problems such as turbulence [42]. However, so far no application to flow in porous media has been reported. Therefore, in the following, a detailed introduction to DMD is given, addressing in particular the porous media community.

A. An introduction to DMD

DMD is a data-driven, i.e., equation-free approach for the analysis of experimental or numerical data [43, 44]. One can consider DMD as a model reduction algorithm but it is actually a way of decomposing dynamic data into individual modes, while making no assumption about the underlying system [43]. While DMD has been originally introduced for data analysis and interpretation in fluid dynamics [41] it has since been applied for many other topics including video processing [45], epidemiology [46], and financial trading [47]. Thus, it is a very general method for the analysis of dynamical systems [48, 49].

The spatial and temporal dynamics that can be extracted from the DMD are linked to the Pollicott-Ruelle resonances [38] which are, in turn, linked to fluid topology [50, 51]. This means that DMD could be applied to multiphase flow in porous media.

For dynamical systems with continuous spectra, the evolution of the system through nonlinear dynamics, can be described using a linear transformation, called the Koopman operator [44, 52, 53]. The Koopman operator represents the evolution via a set of discrete eigenvalues that correspond to stable and unstable modes and their rate of growth or decay.

The advantage is that the state space is represented by a discrete set, whereas, in traditional fluid dynamic studies following the system dynamics via its trajectories in state space results in an infinite number of dimensions. DMD can, under certain conditions, approximate the eigenvalues and eigenvectors of the infinite-dimensional Koopman operator with finite dimensions [43, 44].

In the original application for fluid dynamics, DMD was designed to extract information from flow fields either calculated by computer simulation or experimentally measured [41, 54]. In Figure 1, a high-level overview of the functioning and purpose of DMD for a fluid dynamics application is shown.

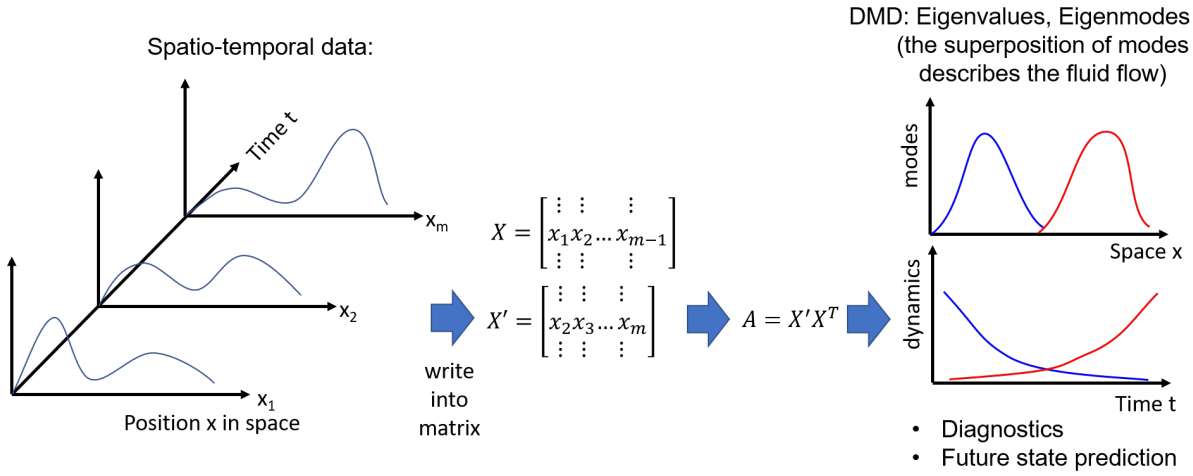

FIG. 1: Application of DMD in fluid dynamics. The spatio-temporal data of an experimentally-measured flow field is cast into a matrix representation which is then decomposed into eigenvalues. These allow to represent the dominant features of the spatio-temporal dynamics with relatively few modes and respective dynamics.

The aim is to represent the system dynamics with a system of extracted modes that have significantly fewer degrees of freedom. This allows a more intuitive description of the underlying physical mechanisms contained in the data sequence. An important aspect is the description of the dynamics within a spatial framework, i.e., the spatio-temporal coupling. The decomposition into modes and respective dynamics can then be used to make predictions about future states [43].

The DMD eigenvalues can also be linked to the Lyapunov exponents. These exponents characterize the relaxation dynamics and rate of energy dissipation. Lyapunov exponents

measure a system's predictability [55, 56]. Extracting this could also help with making future predictions for a given system.

B. The principles of DMD

DMD computes from a time series of data the underlying modes and their respective dynamics such as oscillatory behavior, growth or decay from the eigenvalues of the composition or Koopman operator [42, 44]. The data is generally available in form of a time sequence of snapshots:

$$V_1^N = \{v_1, v_2, ..., v_N\} \tag{1}$$

$v_i \in \mathbb{R}^M$ is the i-th snapshot in the time sequence, and $v_i^N \in \mathbb{R}^{MxN}$ is the data in matrix representation where where the columns contain the individual snapshots.

The dynamics are assumed to be linear, which implies that consecutive snapshots v_i are related to each other via a linear relationship:

$$v_{i+1} = Av_i \tag{2}$$

The assumption of a linear dynamical system furthermore assumes that this linear relationship A remains approximately constant during the time period of interest.

One can re-write Eq. 2 into a matrix form:

$$V_2^N = AV_1^{N-1} + re_{N-1}^T \tag{3}$$

r is the vector of the residuals that account for any possible behavior that cannot be captured by A. $e_{N-1} = \{0, 0, ..., 1\} \in \mathbb{R}^{N-1}$, $V_1^{N-1} = \{v_1, v_2, ..., v_{N-1}\}$, $V_2^N = \{v_2, v_3, ..., v_N\}$.

Dynamic domain composition computes the eigenvalues and eigenvectors of A. For the practical calculation of the eigenvalues of A several different methods are available, where singular value decomposition of A is a central element.

There are several different DMD approaches which have specific advantages and disadvantages [43]. The singular value decomposition (SVD) approach has the advantage that noise in the data can be removed by truncating the SVD of V_1^{N-1}. Furthermore, there are many different types of DMD and such as optimized DMD, optimal mode decomposition, exact DMD, multi-resolution DMD, DMD with Control etc. which have specific strengths

such as multi-resolution DMD for data sets that contain spatial structure at multiple length scales. In this work DMD is performed with `PyDMD` [57] which has several methods. Here we use regular `DMD` for the space-time saturation data. The code for the analysis is provided with this paper.

C. Connection between DMD and Discrete Fourier Transform

A discrete Fourier transform (DFT) projects the time series data x_k on an orthogonal set of harmonic base functions:

$$x_k = \sum_{j=0}^{m} \mu_j^k \hat{x}_j \tag{4}$$

with the harmonic base function expressed in exponential form:

$$\mu_j = e^{\frac{2\pi j}{m+1}} \tag{5}$$

and the Fourier transform $\hat{x_j}$. In the DFT Components $\mu_j = e^{i\phi_j j} = e^{i\omega_j t}$ with frequency ω_j have magnitude 1.

However, DMD eigenvalues are of the form

$$\lambda_j = r_j e^{i\phi_j j} \tag{6}$$

since they are variables, and not necessarily roots of unity. Eigenvalues are characterized by a frequency ω_j and a magnitude r_j, which form a complex frequency [58]. For eigenvalues that are located on the unit cycle, the DMD modes take the form of traveling wave solutions [42]. For general eigenvalues, the DMD eigenvalues are richer because they contain more features of the dynamics such as periodicity, damping or growth etc. The challenge, however, is to identify the relevant DMD components, which is more complicated than in a DFT because in DMD the interplay of eigenvalues λ_j, modes ϑ_j and amplitudes a_j need to be taken into account [58]. Respective strategies to visualize the dominance structure are discussed in [58].

D. DMD Eigenmodes and the Koopman operator

While DMD could be regarded as "yet another decomposition" method, there are more fundamental reasons why DMD could be a meaningful option for the decomposition of dynamic phenomena. There is a fundamental connection between DMD and the Koopman operator [42] which lifts the dynamics of a nonlinar system with finite dimensions into an infinite-dimension space where the dynamics becomes linear. In addition, the Koopman analysis operates in the observable domain. For these reasons, the Koopman analysis has been successfully applied to non-linearities in fluid mechanics [42]. The Koopman eigenfunctions have several advantages over classical spectral analysis which range from the fact that they are discrete and not continuous to practical advantages such as the construction of non-parametric predictors, state estimators and nonlinear controllers using linear systems strategies [44].

In fluid mechanics, the state space is represented by the flow field $\vec{u}$ which evolves according to the Navier-Stokes equation as

$$\partial_t \vec{u}(\vec{x}, t) = \vec{F}(\vec{u}(\vec{x}, t)) \tag{7}$$

g is a complex function on the flow field $\vec{u}$ which represents the state space of the flow. $g(\vec{u})$ produces a complex number for each value of $\vec{u}$ which becomes then an *observable* of flow. The Koopman operator describes the time evolution of this observable. The Koopman operator U at time τ, denoted U^τ maps the function $g(\vec{u}(\vec{x}, t))$ to a new time $t + \tau$ via

$$g(\vec{u}(\vec{x}, t + \tau)) = U^\tau g(\vec{u}(\vec{x}, t)) := g^\tau(\vec{u}(\vec{x}, t)) \tag{8}$$

The Koopman operator U is linear and therefore its spectrum and eigenfunctions provide an intuitive description of the dynamics of the observables. The eigenfunctions of the Koopman operator ϕ_j with eigenvalues λ_j follow

$$\phi^{\tau(\vec{u})} := U^\tau \phi_j(\vec{u}) = e^{\lambda_j \tau} \phi_j(\vec{u}) \tag{9}$$

For periodic, oscillatory phenomena the eigenvalues are

$$\lambda_j = i\omega_j, \ \omega_j \in \mathbb{R} \tag{10}$$

which establishes a connection between the Koopman eigenvalues and the frequency spectrum.

Observables can now be expressed through linear combinations of the eigenfunctions

$$g(\vec{u}) = \sum_{j=1}^{\infty} g_j \phi_j(\vec{u}) \tag{11}$$

where the scalar coefficients g_j are defined by the projection of the observable g on the Koopman eigenfunction ϕ_j. Using eq. 8 the time evolution of the observable g can be expressed in terms of the Koopman eigenfunctions

$$g^{\tau}(\vec{u}) = U^{\tau} g(\vec{u}) = \sum_{j=1}^{\infty} g_j \phi_j(\vec{u}) e^{i\omega_j \tau} \tag{12}$$

The same principle holds also for vector observables $\vec{g}$

$$\vec{g}^{\tau}(\vec{u}) = U^{\tau} \vec{g}(\vec{u}) = \sum_{j=1}^{\infty} \vec{g}_j \phi_j(\vec{u}) e^{i\omega_j \tau} \tag{13}$$

$\vec{g}_j$ describes the components of the observable $\vec{g}$ obtained by projection on the Koopman eigenfunction ϕ_j [44]. The respective decomposition of observables into Koopman eigenfunctions is termed Koopman Mode Decomposition (KMD) [44]. $\vec{g}_j$ are the Koopman modes associated with the Koopman eigenvalue λ_j for in this case $\lambda_j = i\omega_j$ i.e. with Koopman frequency ω_j. Effectively the time-evolution of $\vec{g}$ is a linear combination of Koopman modes with oscillating coefficients. Note that since the expansion in eq. 13 is infinite dimensional, it can also describe nonlinear time evolution [44].

This makes DMD a physically-rooted data-driven approach linked to spectral decomposition of the Hamiltonian dynamics in contrast to an arbitrary data-driven approaches entirely based on correlations without any comprehensive physical meaning.

E. DMD applied to analyzing experimental data on multiphase flow in porous media

The connection between DMD eigenmodes, the Koopman operator, Ruelle-Pollicott resonances and topological properties suggests DMD could be utilised to extract topology and characteristic time from complex signals [50]. These are typical for multi-phase flow through

porous media due to the interaction of multiple fluids with a highly heterogeneous pore space leading to a range of fluid flow phenomena such as ganglion dynamics, fluid front instabilities, intermittent flow pathways [9, 20, 27, 59–63]. DMD is also an equation-free method, and is also applicable to stochastic-statistical dynamical systems [43, 64]. This further emphasises its use in analyzing data sets such as fluctuations observed during two-phase fractional flow in porous media.

DMD can, under specific conditions, compute the Koopman eigenmodes. The normal modes of periodic dynamics such as linear oscillations can be equally-well represented in a non-linear dynamics by their Koopman modes [54].

To understand how well DMD can reproduce the data, and the extent it improves our understanding of complex two-phase flow dynamics, we take two data sets. The first data set [27], referred to as case 1, has a fluid front instability. When looking at the saturation data in space and time, there are clear waves as the front advances. This is useful for understanding how well DMD reconstructs data as it is a clear indicator to the quality of the reconstruction. We can then pick the modes associated with the largest magnitude eigenvalues, and assess how many modes are required to reconstruct the data.

The other data set, referred to as case 2, looks at intermittent flow pathways [61]. As the capillary number increases, the amount of intermittent flow pathways increases, leading to complex dynamics as multiple connection and disconnection events occur at the same time. However, in this data set, at the lowest capillary number, there is a unique configuration where one pore controls connection across the pore space in the middle of the core. This singular pore periodically disconnects and reconnects, and these events are heavily influence the pressure and saturation data. To observe this in the DMD would be further evidence on how well DMD can represent the data. But to then apply to the higher capillary numbers will allow us to ascertain if DMD can pick up dynamics that cannot be observed in other ways such as through saturation or pressure data alone.

III. RESULTS AND DISCUSSION

A. The reproduction of dynamic flow features using DMD

The first data set comprises of steady-state two-phase flow experiments where oil and brine were injected simultaneously into a cylindrical sandstone sample with a diameter of 2.54 cm and a length of 4.45 cm at different fractional flows. The full experimental procedure is discussed in [27]. X-ray imaging was used to obtain the saturation profile across the core at steady-state. Steady-state was determined by the pressure drop measured across the sample; at steady-state there are still fluctuations in the pressure data (as shown in Figure 2 B and D), but when averaged in time, the pressure remains constant.

The water saturation in these experiments had a peak that moved across the rock sample at a constant velocity. This formed a travelling wave, indicated by the red streaks, indicating higher saturation, shown in Figure 2 A and C. The nature of the travelling wave front changed depending on the fractional flow i.e. the slope of the streak changes between Figure 2 A and B. This distinctive feature allows us to qualitatively assess the reconstruction power of DMD.

The DMD of saturation data gives 24 eigenvalues, with the 8 largest eigenvalues highlighted in Figure 3. These are plotted in space and time as the respective modes and dynamics of the flow. Some are purely real numbers (e.g. #0 and #1), some are reflected in the x axis (e.g. #2 is a reflection about the x axis of #3). Overall, there is a wealth of dynamics in the DMD that should correspond to flow dynamics. The superposition of all the modes and dynamics should, in principle, recreate the data set input into the DMD (as long as the DMD has a long enough time series as an input).

Taking all modes and dynamics, the DMD is capable of reconstructing the initial data, shown in Figure 4 B). When the modes are reconstructed separately, they represent different parts of the flow regime, highlighted in Figure 5. The question is how many modes and their corresponding dynamics are required to reconstruct the data sufficiently, and represent the larger scale flow properties? We take the first 4 modes and 4 dynamics (shown in Figure 3) and reconstruct the data set (shown in Figure 4 C). This can recreate the travelling wave front sufficiently well.

Overall, DMD is capable of preserving the flow signal so that it can be reconstructed. Not

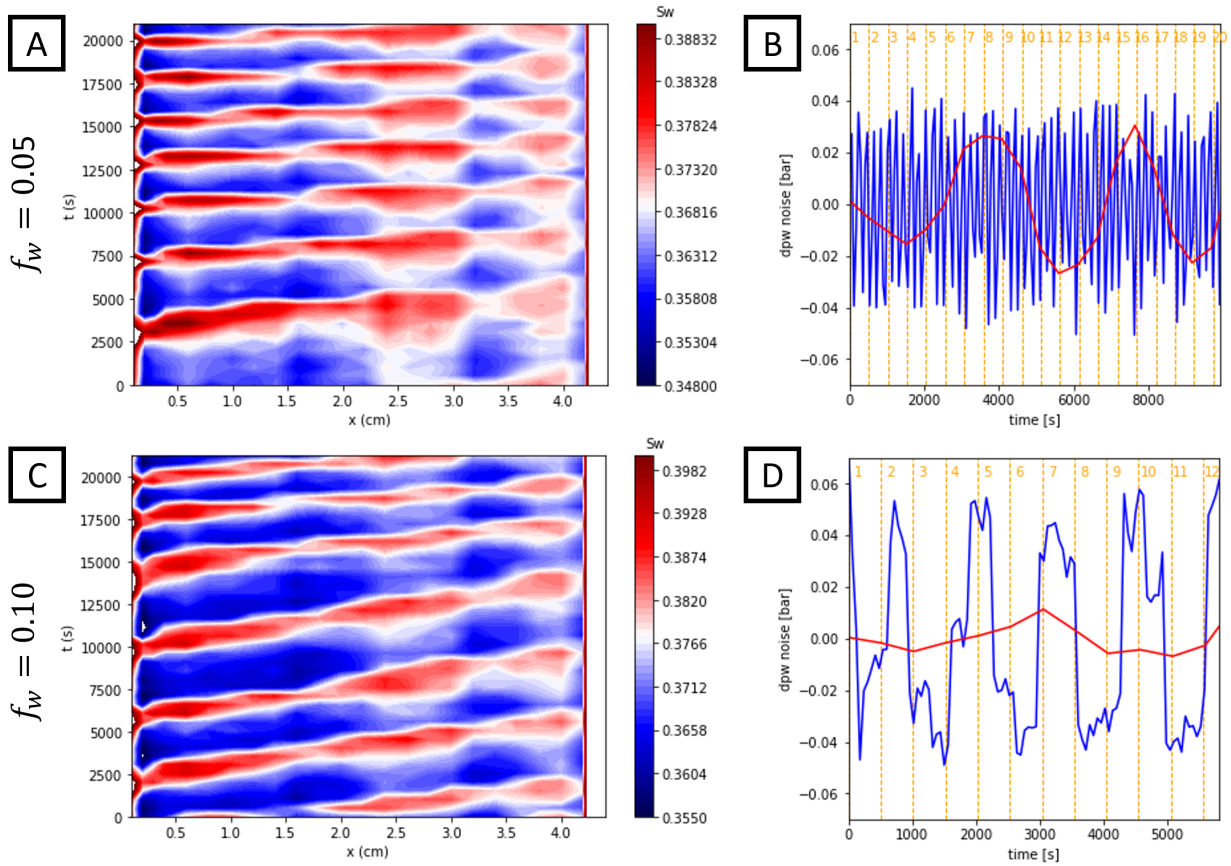

FIG. 2: Saturation and pressure for steady-state experiment showing oscillatory behavior of saturation and pressure drop caused by a fractional flow instability that involves hysteresis. A) Contour plot of saturation vs. space and time for fractional flow $f_w = 0.05$ and B) average saturation (red) and pressure drop (blue) as a function of time. C-D) same as A-B) but for fractional flow $f_w = 0.10$. The saturation countour plots A,C show clearly the travelling wave behavior caused by the instability. Data taken from [27]

all modes and dynamics are needed to preserve the large scale flow features. The number of modes and dynamics required to reconstruct the data could reflect the complexity of the dynamics, and the extent of the interaction between fluids. However, a measure to how well a signal has been reconstructed is easier to deduce when there are clear, periodic instabilities, such is the case in this example.

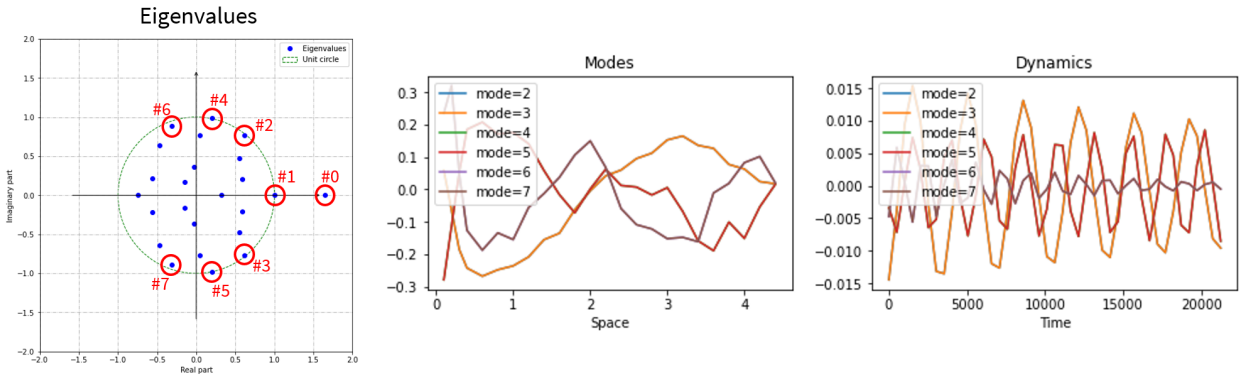

FIG. 3: A) the eigenvalues from the DMD for $f_w = 0.10$, with the 8 largest magnitude eigenvalues circled and numbered. B) corresponding modes in space for the 8 largest eigenvalues from the DMD. C) corresponding dynamics in time for the 8 largest eigenvalues from the DMD.

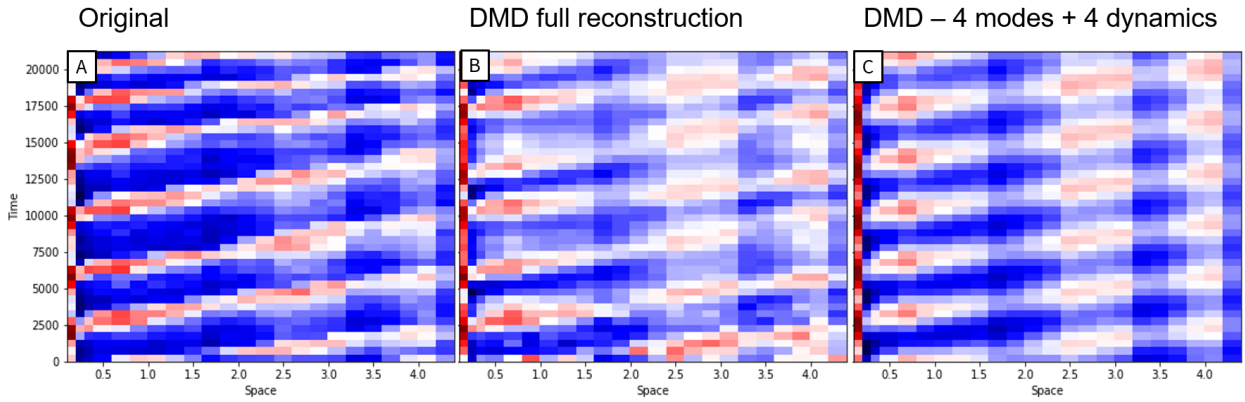

FIG. 4: A) original input data showing the saturation in time (s) and space (cm), B) DMD full reconstruction of the original input data, and C) DMD reconstruction from the 4 largest modes (modes 1-4 in Figure 3) and their corresponding dynamics.

B. Identifying the control of localised heterogeneity on flow dynamics using DMD

Recently, a wealth of dynamics has been observed in steady-state fluid flow due to the interaction of multiple fluids through the heterogeneous network of pores in rocks [27, 28, 60–62]. The dynamics are difficult to unravel due to the heterogeneity of the porous medium, and the non-local nature of the dynamics [61]. We want to observe if DMD can provide a deeper insight into these dynamics.

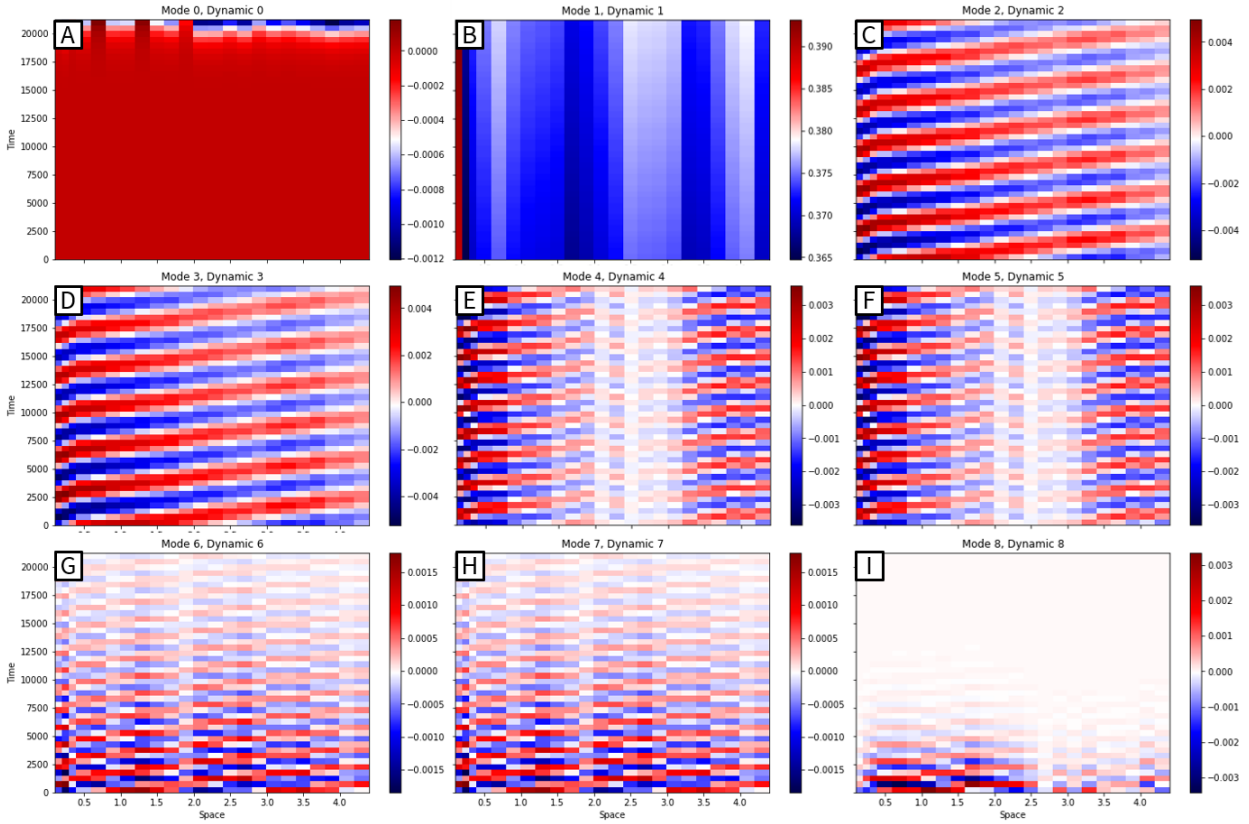

FIG. 5: DMD reconstruction done separately for the 8 largest eigenvalues in Figure 3.

To explore this we examine a series of two-phase steady-state experiments where nitrogen and brine were simultaneously injected into a cylindrical carbonate sample with a diameter of 21 mm and a length of 5 mm at a fractional flow of 0.85, with the total flow rate increased from 0.1ml/min to 0.7ml/min. The images were acquired over a period of 1s, with the full experimental procedure discussed in [61]. This example is useful for this analysis because at the lowest flow rate/ capillary number, the flow is channelled through a single pore that intermittently connects and disconnects. This created a strong periodic pressure signal; something that is translated, although not simply, into the saturation across the sample, as shown in Figure 6. As the flow rate increased, the gas distribution became more evenly distributed across the sample. There are more intermittent dynamics at these higher flow rates, and this combined with the non-local nature of the signal, creates a more complicated pressure signal (Figure 6 E and F). It is then harder to correlate specific events in the pore space to pressure fluctuations across the core.

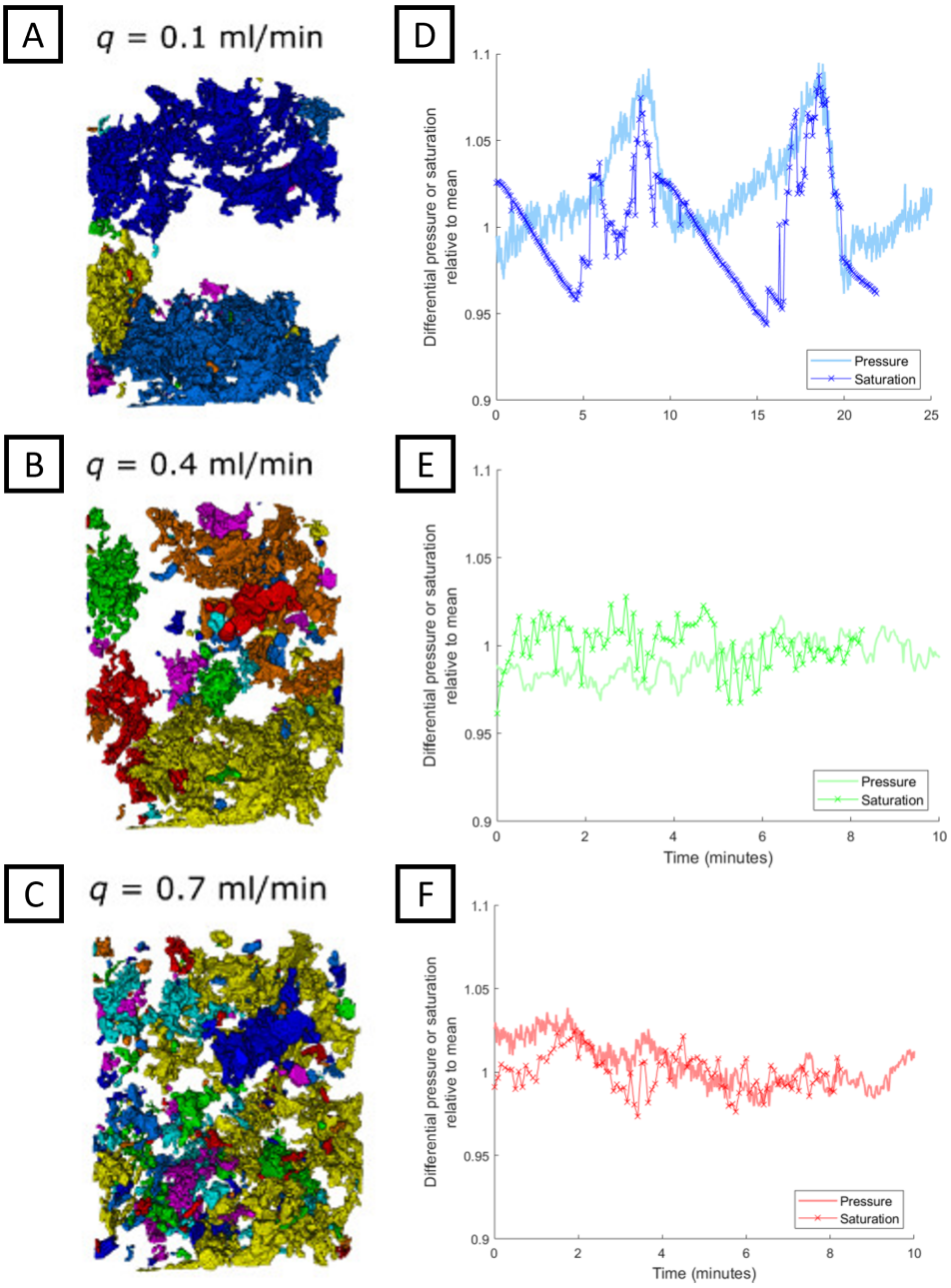

FIG. 6: A-C) Gas ganglion distribution shown for the different flow rates (each colour denotes a distinct region of gas), and D-F) pressure and saturation readings, relative to the mean, for the different flow rates. Note that there are many more data points for pressure than saturation due to differences in recording intervals.

The DMD of the lowest capillary number shows modes with a node at the middle of the sample, which is where the one pore constriction occurs. This region is highlighted for the

higher flow rate experiments in Figure 7. For the middle flow rate, there is still a divide in the modes downstream of the constriction, compared to upstream. For the highest flow rate, there are peaks in the modes for the middle section.

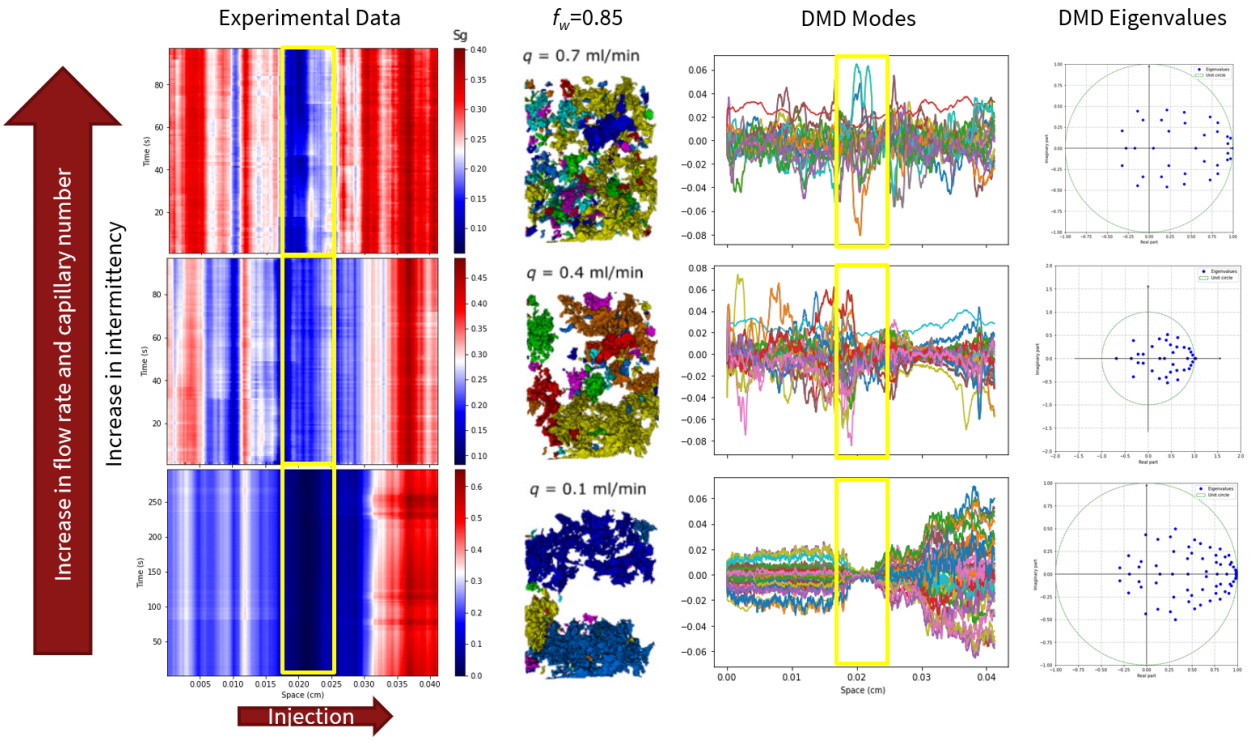

FIG. 7: The experimental data (shown as saturation in space and time). The modes from the DMD analysis and the corresponding eigenvalues. The yellow boxes in the experimental data highlights the central region of the sample, where there is only 1 pore connecting flow across the sample for the lowest flow rate. This connection is evident in the DMD mode where a node is formed in the yellow box where this connection occurs.

This middle section of the core is highly heterogeneous, which caused the channelling of the flow during the lowest flow rate observation. This section still has a large influence on dynamics, even when energy dissipation from intermittent pathway flow becomes more disperse, as shown by the DMD. Overall, DMD was able to provide a better insight into the dynamics in more complex scenarios. It provides a way to assess fluctuations in data sets that are not periodic and, therefore, obvious to spot with the naked eye.

C. Sampling intervals and their impact on DMD

Temporal resolution is typically a restraining factor when conducting multi-phase flow experiments [60, 65]. The experiments used in this work were conducted at synchrotron facilities, where high energy X-rays are generated; these cannot be achieved in traditional laboratory based experiments. To assess the universality of DMD on the experimental data currently in the domain, we must ascertain how long a time series (and the sampling interval) is required for the DMD to accurately represent the flow properties.

We vary the sampling interval for the case 2, lowest capillary number example from 2 s to 1 minute. The node in the modes is visible for sampling up to every 32s (Figure 8 e). Recording the dynamics every 64s does not provide enough data to capture the node in the dynamics in the middle of the sample. However, it is captured for a sampling interval of 32 s. This suggests that rapid imaging is acquired to observed the relevant flow dynamics, and typical laboratory based X-ray scanners, which take 10s of minutes, are an order of magnitude too slow to capture the relevant dynamics.

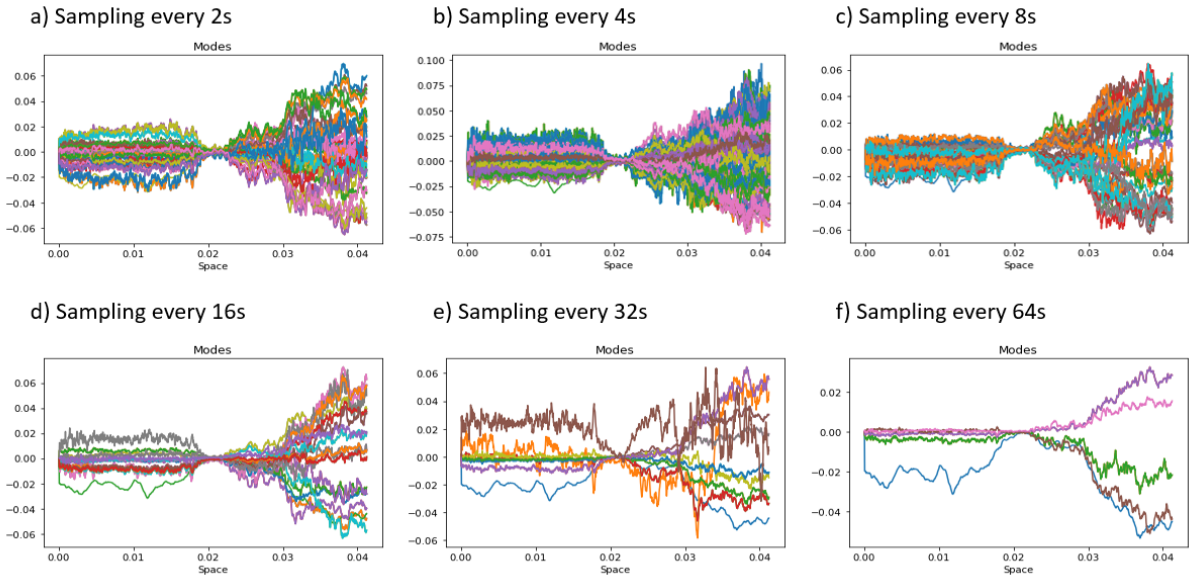

FIG. 8: Modes for the lowest capillary number experiment in case 2 with different sampling times varying from 2s to 64s. The sampling time is the gap between scanning interval, with the duration of a scan remaining constant, at 1s.

D. Can we link saturation DMD results to red noise observed in the pressure data?

As shown in Figure 8, the number of modes decreases as the sampling time increases. This means that there are modes with shorter timescales, and those that have longer timescales. In recent work exploring fluctuations in pressure data, red noise was observed [66]. This observation implies a cascade of timescales, with the longer timescales correlating to larger events.

We explore how the nature of the eigenvalues as the sampling interval changes for the lowest capillary number experiment in case 2 (Figure 3 A)). The eigenvalues for this experiment are plotted in Figure 9: the black circle denotes the unit circle. All eigenvalues are stable, so lie within the unit circle. Eigenvectors with magnitudes of > 95 % of the unit circle are classified as periodic. Eigenvalues with magnitudes different than 1 are associated with non-periodic eigenvectors and their modes are either decaying or growing. No eigenvalues lie outside the unit circle, therefore no modes are growing. The number of periodic eigenvalues decreases as the sampling interval increases. The number of eigenvalues decreases, (disproportionately affecting the periodic eigenvalues) but eigenvalues that would have previously been considered periodic, become non-periodic, with a longer sampling interval. This is clearest between Figure 9 e) and f) where non-periodic solutions appear where there was no periodic solution before.

A summary of all the eigenvalues' relationship with the sampling time for all capillary numbers is shown in Figure 10. For all cases, the periodic eigenvalues decay quicker than the non-periodic eigenvalues (shown in the top panel). The total number of eigenvalues decays, along with their magnitude in the middle and bottom panels, respectively. The slope for the lines of best fit varies slightly between capillary numbers, but with no obvious trend.

As some eigenvalues change from being periodic to non-periodic, it is difficult to track a specific mode in time, and observe what it does. This is something that could be of interest in future work.

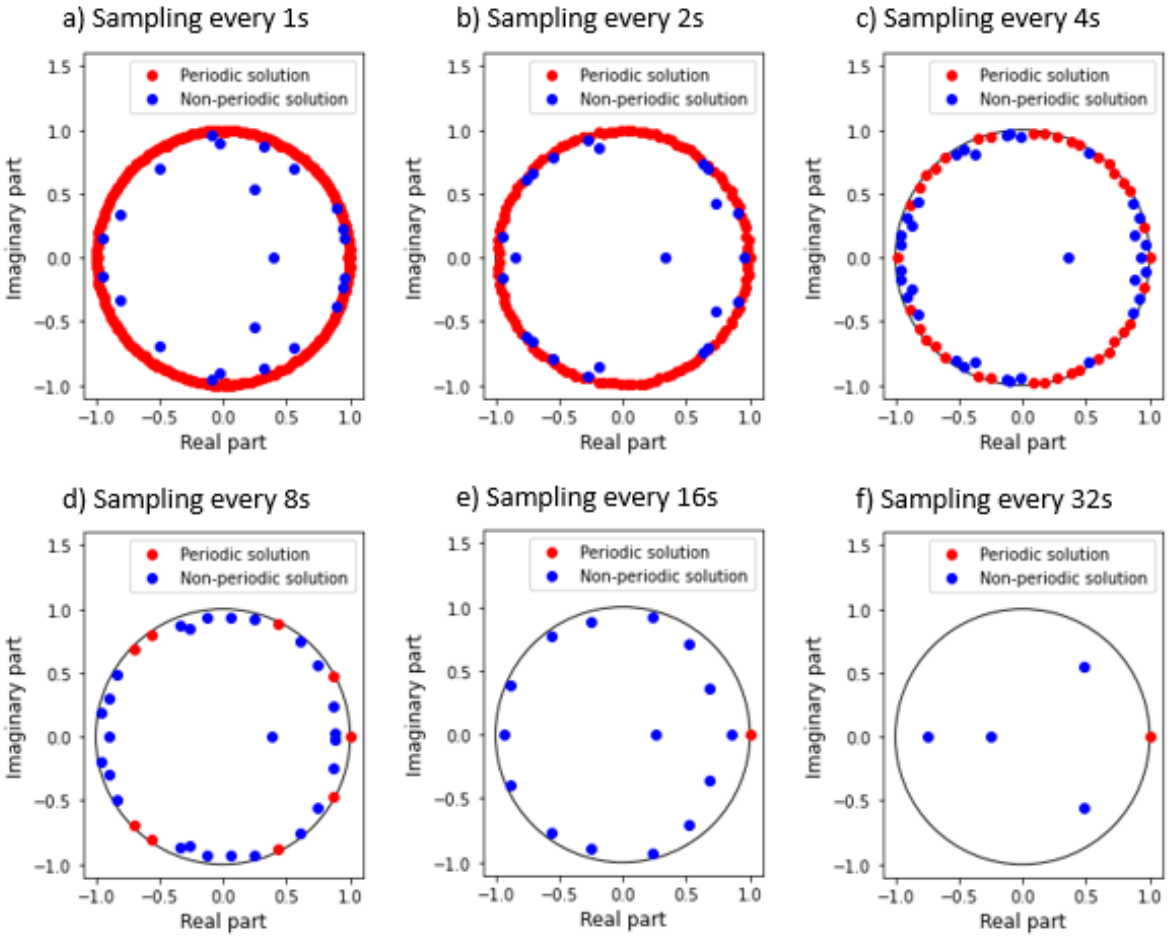

FIG. 9: Eigenvalues for the different sampling intervals. The black circle denotes the unit circle. All eigenvalues are stable, so lie within the unit circle. Eigenvectors with magnitudes of > 95 % of the unit circle are classified as periodic. Eigenvalues with magnitudes different than 1 are associated with non-periodic eigenvectors and their modes are either decaying or growing.

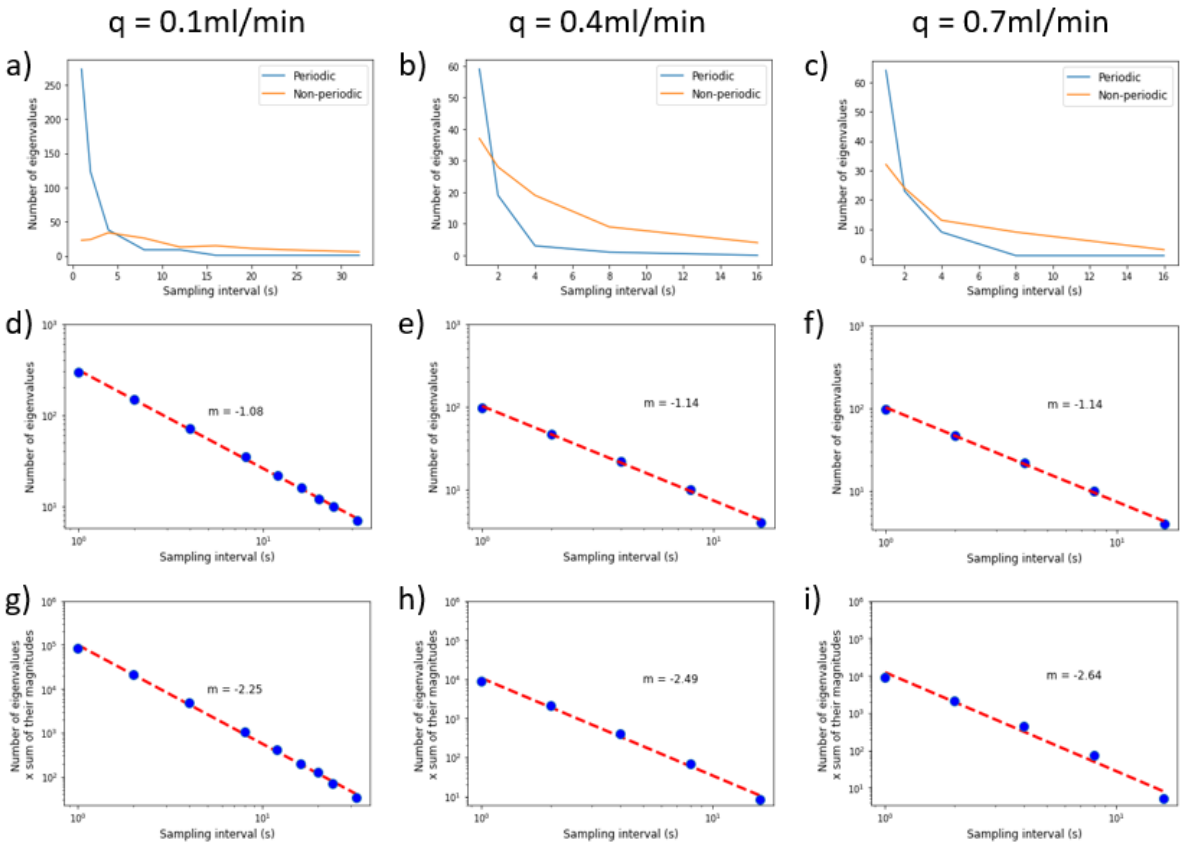

FIG. 10: Top panel: the number of eigenvalues for periodic and non-periodic solutions for different sampling intervals for all capillary numbers in case 2. Middle panel: the total number of eigenvalues for different sampling intervals for all capillary numbers in case 2. For the bottom panel, the dashed red line shows the line of best fit, with the slope, m, listed. Bottom panel: the total number of eigenvalues multiplied by the sum of their magnitude for different sampling intervals for all capillary numbers in case 2.

IV. CONCLUSIONS

In this work we show that dynamic mode decomposition (DMD) is a useful tool for analysing the flow dynamics for multi-phase flow in porous media.

The fluctuations shown in saturation data can be extracted from the DMD eigenvalues. We show that the associated modes and dynamics from the output can be used to reconstruct the input data. More so, not all modes and dynamics are required to successfully reconstruct the large scale features. Thus, DMD could be used as a tool for understanding which dynamics are important for larger scale flow properties, and could be useful in upscaling attempts.

We observed that DMD can successfully highlight regions controlling flow, and provide insight into the flow dynamics, when the number of fluctuations/ amount of dynamics makes it difficult to qualitatively describe flow.

Future work will explore if saturation DMD could be linked with fluctuations in pressure data. There is the potential to link the DMD analysis with a Fourier analysis or power spectra analysis.

DMD could potentially be used to process large amounts of 4D data, which is typical for synchrotron imaging of flow in porous media. The DMD analysis could be expanded to have the raw projections as the input. From this, the dominant modes and their timescales could be extracted and this could be used to find the correct reconstruction parameters. This could be paired with machine learning to provide an efficient and robust way to process 4D data.

V. DATA AVAILABILITY

The code to perform a dynamic mode decomposition on saturation profiles with time is available on github: https://github.com/cspurin/DMD

[1] M. Muskat, Soil Science **46**, 169 (1938).

[2] J. Bear, *Dynamics of fluids in porous media* (Courier Corporation, 1988).

[3] R. Lenormand, C. Zarcone, and A. Sarr, Journal of Fluid Mechanics **135**, 337 (1983).

[4] V. Joekar-Niasar and S. Hassanizadeh, Critical reviews in environmental science and technology **42**, 1895 (2012).

[5] M. J. Blunt, *Multiphase Flow in Permeable Media: A Pore-Scale Perspective* (Cambridge University Press, 2017).

[6] M. J. Blunt, M. D. Jackson, M. Piri, and P. H. Valvatne, Advances in Water Resources **25**, 1069 (2002).

[7] A. Ferrari and I. Lunati, Advances in water resources **74**, 1 (2014).

[8] D. Avraam and A. Payatakes, Journal of Fluid Mechanics **293**, 207 (1995).

[9] M. Rücker, S. Berg, R. Armstrong, A. Georgiadis, H. Ott, A. Schwing, R. Neiteler, N. Brussee, A. Makurat, L. Leu, *et al.*, Geophysical Research Letters **42**, 3888 (2015).

[10] S. Schlüter, S. Berg, M. Rücker, R. T. Armstrong, H. Vogel, R. Hilfer, and D. Wildenschild, Water Resources Research **52**, 2194 (2016).

[11] J. E. McClure, R. T. Armstrong, M. A. Berrill, S. Schlüter, S. Berg, W. G. Gray, and C. T. Miller, Phys. Rev. Fluids **3**, 084306 (2018).

[12] H. Hadwiger, *Vorlesung über Inhalt, Oberfläche und Isoperimetrie* (Springer, 1957).

[13] A. L. Herring, E. J. Harper, L. Andersson, A. Sheppard, B. K. Bay, and D. Wildenschild, Advances in Water Resources **62**, 47 (2013).

[14] C. Miller, K. Bruning, C. Talbot, J. McClure, and W. Gray, Water Resources Research **55**, 6825 (2019).

[15] M. Rücker, W.-B. Bartels, G. Garfi, M. Shams, T. Bultreys, M. Boone, S. Pieterse, G. Maitland, S. Krevor, V. Cnudde, *et al.*, Journal of colloid and interface science **562**, 159 (2020).

[16] C. Sun, J. McClure, P. Mostaghimi, A. L. Herring, D. E. Meisenheimer, D. Wildenschild, S. Berg, and R. T. Armstrong, Journal of Colloid and Interface Science **578**, 106 (2020).

[17] J. E. McClure, T. Ramstad, Z. Li, R. T. Armstrong, and S. Berg, Transport in Porous Media **133**, 229 (2020).

[18] R. T. Armstrong, H. Ott, A. Georgiadis, M. Rücker, A. Schwing, and S. Berg, Water Resources Research **52**, 9162 (2014).

[19] S. Schlüter, S. Berg, T. Li, H. Vogel, and D. Wildenschild, Water Resources Research **53**, 4709 (2017).

[20] C. Spurin, T. Bultreys, B. Bijeljic, M. J. Blunt, and S. Krevor, Physical Review E **100**, 043103 (2019).

[21] H. Darcy, *Les fontaines publiques de la ville de Dijon: Exposition et application des principes à suivre et des formules à employer dans les questions de distribution d'eau: Ouvrage terminé par un appendice relatif aux fournitures d'eau de plusieurs villes, au filtrage des eaux et à la fabrication des tuyaux de fonte, de plomb, de tôle et de bitume*, Vol. 2 (V. Dalmont, 1856).

[22] S. Hassanizadeh and W. Gray, Advances in Water Resources **16**, 53 (1993).

[23] Z. Liu, A. Herring, C. Arns, S. Berg, and R. T. Armstrong, Transport in Porous Media **118**, 99 (2017).

[24] S. Khorsandi, L. Li, and R. T. Johns, SPE Journal **22**, 1915 (2017).

[25] J. E. McClure, S. Berg, and R. T. Armstrong, Archivx (2019).

[26] A. Hansen, E. G. Flekkøy, S. Sinha, and P. A. Slotte, arXiv , 2205.13791 (2022).

[27] M. Rücker, A. Georgiadis, R. T. Armstrong, H. Ott, N. Brussee, H. Van der Linde, L. Simon, F. Enzmann, M. Kersten, and S. Berg, Frontiers in Water **3**, 671399 (2021).

[28] Y. Gao, Q. Lin, B. Bijeljic, and M. J. Blunt, Water Resources Research **53**, 10274 (2017).

[29] Y. Gao, A. Q. Raeini, M. J. Blunt, and B. Bijeljic, Advances in Water Resources **129**, 56 (2019).

[30] H. Menke, Y. Gao, S. Linden, and M. Andrew, Frontiers in Water **4**, 935035 (2022).

[31] S. S. Datta, T. Ramakrishnan, and D. A. Weitz, Physics of Fluids **26**, 022002 (2014).

[32] Y. Wang and S. K. Masalmeh, in *E3S Web of Conferences*, Vol. 89 (EDP Sciences, 2019) p. 02007.

[33] J. E. McClure, S. Berg, and R. T. Armstrong, Phys. Rev. E **104**, 045106 (2021).

[34] J. E. McClure, S. Berg, and R. T. Armstrong, Physics of Fluids **33**, 083323 (2021).

[35] J. E. McClure, M. Fan, S. Berg, R. T. Armstrong, C. F. Berg, Z. Li, and T. Ramstad, Physics of Fluids **34**, 092011 (2022).

[36] D. Bedeaux and S. Kjelstrup, Entropy **24**, 46 (2021).

[37] D. C. Standnes, D. S. Sleveland, and A. Kristoffersen, Transport in Porous Media , 1 (2022).

[38] D. Ruelle, Physical Reivew Letters **56**, 405 (1986).

[39] S. Viscardy, arXiv , cond (2006).

[40] M. Winkler, M. A. Gjennestad, D. Bedeaux, S. Kjelstrup, R. Cabriolu, and A. Hansen, Frontiers in Physics **8**, 60 (2020).

[41] P. J. Schmid, Journal of Fluid Mechanics **656**, 5 (2010).

[42] A. S. Sharma, I. Mezić, and B. J. KcKeon, Physical Review Fluids **1**, 032402(R) (2016).

[43] J. N. Kutz, S. L. Brunton, B. W. Brunton, and J. L. Proctor, *Other Titles in Applied Mathematics: Dynamic Mode Decomposition: Data-Driven Modeling of Complex Systems* (Society of Industrial and Applied Mathematics, 2016).

[44] H. Arabi and I. Mezić, SIAM J. Applied Dynamical Systems **16**, 2096 (2017).

[45] C. Bi, Y. Yuan, J. Zhang, Y. Shi, Y. Xiang, Y. Wang, and R. Zhang, IEEE Access **6**, 21397 (2018).

[46] D. Bistrian, G. Dimitriu, and I. Navon, in *AIP Conference Proceedings*, Vol. 2164 (AIP Publishing LLC, 2019) p. 080002.

[47] J. Mann and J. N. Kutz, Quantitative Finance **16**, 1643 (2016).

[48] P. J. Schmid, Annual Review of Fluid Mechanics **54**, 225 (2022).

[49] J. N. Kutz, S. L. Brunton, B. W. Brunton, and J. L. Proctor, *Dynamic mode decomposition: data-driven modeling of complex systems* (SIAM, 2016).

[50] B. Küster and T. Weich, Commun. Math. Phys. **378**, 917 (2020).

[51] S. Dyatlov and M. Zworski, Inventiones mathematicae **210**, 211 (2017).

[52] B. O. Koopman, Proc. Natl. Acad. Sci. USA **17**, 315 (1931).

[53] B. O. Koopman and J. van Neumann, Prof. Natl. Acad. Sci. USA **18**, 255 (1932).

[54] I. Mezić, Annual Review of Fluid Mechanics **45**, 357 (2013).

[55] A. Wolf, J. B. Swift, H. L. Swinney, and J. A. Vastano, Physica D: nonlinear phenomena **16**, 285 (1985).

[56] B. Cessac, P. Blanchard, and T. Krüger, Physical Review E **64**, 016133 (2001).

[57] N. Demo, M. Tezzele, and G. Rozza, The Journal of Open Source Software **3**, 530 (2018).

[58] T. Krake, S. Reinhardt, M. Hlawatsch, B. Eberhardt, and D. Weiskopf, Visual Informatics **5**, 15 (2021).

[59] C. Spurin, T. Bultreys, B. Bijeljic, M. J. Blunt, and S. Krevor, Physical Review E **100**, 043115 (2019).

[60] C. Spurin, T. Bultreys, M. Rücker, G. Garfi, C. M. Schlepütz, V. Novak, S. Berg, M. J. Blunt, and S. Krevor, Water Resources Research **56**, e2020WR028287 (2020).

[61] C. Spurin, T. Bultreys, M. Rücker, G. Garfi, C. M. Schlepütz, V. Novak, S. Berg, M. J. Blunt, and S. Krevor, Advances in Water Resources **150**, 103868 (2021).

[62] C. A. Reynolds, H. Menke, M. Andrew, M. J. Blunt, and S. Krevor, Proceedings of the National Academy of Sciences **114**, 8187 (2017).

[63] Y. Gao, Q. Lin, B. Bijeljic, and M. J. Blunt, Physical Review Fluids **5**, 013801 (2020).

[64] M. D. Chekroun, A. Tantet, H. A. Dijkstra, and J. D. Neelin, Journal of Statistical Physics **179**, 1366 (2020).

[65] Y. Gao, A. Q. Raeini, M. J. Blunt, and B. Bijeljic, Physical Review E **103**, 013110 (2021).

[66] C. Spurin, M. Rücker, M. Moura, T. Bultreys, G. Garfi, S. Berg, M. J. Blunt, and S. Krevor, Water Resources Research **58**, e2022WR031947 (2022).